# Phase transition kinetics revealed by *in situ* x-ray diffraction in laser-heated dynamic diamond anvil cells

Matthew Ricks, Arianna E. Gleason, Francesca Miozzi, Hong Yang, Stella Chariton, Vitali B. Prakapenka, Stanislav V. Sinogeikin, Richard L. Sandberg, Wendy L. Mao, and Silvia Pandolfi, Logarithment of Physics and Astronomy, Brigham Young University, Provo, Utah 84602, USA

1 Department of Physics and Astronomy, Brigham Young University, Provo, Utah 84602, USA

2 SLAC National Accelerator Laboratory, 2575 Sand Hill Rd., Menlo Park, California 94025, USA

3 Earth and Planets Laboratory, Carnegie Institution for Science, Washington, DC 20015, USA

4 Department of Earth and Planetary Sciences, Stanford University, 450 Jane Stanford Way, Building 320, Stanford, California 94305, USA

5 Center for Advanced Radiation Sources, The University of Chicago, Chicago, Illinois 60637, USA

6 DAC Tools, LLC, Naperville, Illinois 60565, USA

7 Sorbonne Université, Muséum National d'Histoire Naturelle, UMR CNRS 7590, Institut de Minéralogie,

(Received 23 June 2023; accepted 29 January 2024; published 22 March 2024)

de Physique des Matériaux et de Cosmochimie, IMPMC, 75005 Paris, France

We report successful coupling of dynamic loading in a diamond anvil cell and stable laser heating, which enables compression rates up to 500 GPa/s along high-temperature isotherms. Dynamic loading in a diamond-anvil cell allows exploration of a wider range of pathways in the pressure-temperature space compared to conventional dynamic compression techniques. By *in situ* x-ray diffraction, we are able to characterize and monitor the structural transitions with the appropriate time resolution i.e., millisecond timescales. Using this method, we investigate the  $\gamma$ - $\epsilon$  phase transition of iron under dynamic compression, reaching compression rates of hundreds of GPa/s and temperatures of 2000 K. Our results demonstrate a distinct response of the  $\gamma$ - $\epsilon$  and  $\alpha$ - $\epsilon$  transitions to the high compression rates achieved, possibly due to the different transition mechanisms. These findings open up new avenues to study tailored dynamic compression pathways in the pressure-temperature space and highlight the potential of this platform to capture kinetic effects (over ms time scales) in a diamond anvil cell.

## DOI: 10.1103/PhysRevResearch.6.013316

#### I. INTRODUCTION

Understanding how matter responds and deforms under a wide range of compression rates is crucial for various fields, from planetary formation modeling [1] to high-strength ceramic development [2]. Dynamic compression experiments generally rely on the generation and propagation of supersonic shock waves to reach extreme pressure and temperature (P-T) conditions; single-shock experiments, however, are constrained to probe states along the Principal Hugoniot of a material [3]. Here, we successfully demonstrate the use of a dynamic-diamond anvil cell (dDAC) setup compatible with in situ laser heating (LH). This setup enables rapid (ms) isothermal compression at high temperature (HT), significantly expanding the range of conditions that can be studied at high compression rates. We use *in situ* x-ray diffraction (XRD) to study the phase transitions of iron (Fe), and demonstrate compression rates of hundreds of GPa/s at temperatures up to 2000 K. By accessing this largely unexplored region of

Published by the American Physical Society under the terms of the Creative Commons Attribution 4.0 International license. Further distribution of this work must maintain attribution to the author(s) and the published article's title, journal citation, and DOI.

compression rates, we provide valuable experimental insight lacking in this regime, especially at high temperature.

Fe is the main constituent of the Earth's core; as such, its behavior at extreme conditions has been extensively studied, both experimentally and theoretically. The stable structure of Fe at ambient conditions, the so-called  $\alpha$  phase with bodycentered cubic (bcc) structure, transforms into an hexagonal-close packed (hcp) structure, the  $\epsilon$  phase, under high pressure (HP) [4]. The HT phase,  $\gamma$ , has a face-centered cubic (fcc) structure. Upon compression, this phase transforms into the  $\epsilon$  phase, which remains stable up to multi-mbar pressures and is believed to be present in the Earth's solid core [5,6].

Numerous static compression experiments have investigated Fe behavior at HP-HT [4,7–15]. To characterize the equilibrium phase diagram and reproduce more accurately the conditions in Earth's interior, efforts were made in these studies to maintain quasihydrostatic conditions. On the other hand, conventional dynamic compression techniques, such as gas gun and laser ablation, have been used to characterize Fe deformation and melting at ultrafast timescales, from  $\mu$ s down to ps [16–27]. These techniques can attain pressures up to several TPa [28]; however, they are constrained to probe specific thermodynamic pathways in the P-T space. The Principal Hugoniot of Fe crosses the  $\alpha$ - $\epsilon$  phase boundary, and the transition under shock and ramp compression has been observed at higher pressures than the value from

static compression experiments [29–32]. Despite recent developments that allow us to deploy more complex, off-Hugoniot compression profiles [33–35], the  $\gamma$ - $\epsilon$  transition remains inaccessible using conventional dynamic compression techniques.

Recent developments in dDAC technology allow exploration of intermediate compression timescales in between conventional static compression experiments performed over minutes to hours, and shock compression experiments that generate uniaxial compression states over microseconds to nanoseconds. Using either gas supplied membranes or electromechanical piezoelectric actuators to control pressure, dDACs can access compression rates up to 160 TPa/s [36,37]. Konôpková et al. investigated the  $\alpha$ - $\epsilon$  transition of Fe at compression rates up to 4.1 GPa/s at 300 K, and found a transition onset consistent with the quasiequilibrium phase diagram when experiments were conducted in quasihydrostatic conditions [38]. Here, we use a double-sided LH-compatible dDAC that enables simultaneous heating and compression to extend previous studies and explore Fe phase transitions up to 500 GPa/s and 2000 K. With this capability, we provide the insight into the  $\gamma$ - $\epsilon$  phase transition of Fe under compression over millisecond timescales. We report a different response to increasing compression rates for the  $\alpha$ - $\epsilon$  and  $\gamma$ - $\epsilon$  phase transitions, respectively, and ascribe it to the specifics of the transition mechanism at the atomic level. Our findings demonstrate a dDAC platform compatible with laser heating HT experiments which enables in situ characterization of structural transformations over millisecond timescales at varying compression rates and temperatures.

## II. EXPERIMENTAL METHOD

Experiments were conducted at the 13-IDD beamline of the GSECARS sector of the Advanced Photon Source [39]. Compression was performed in a mini-BX80 DAC equipped with a membrane enclosure for remote control of the pressure and with an intermediate buffer for fast loading [36]. The short working distance of the apparatus is compatible with the double-sided laser heating setup of the 13-IDD beamline [40], and allowed for isothermal dynamic compression runs at HT (Fig. 1, see also Sec. I of the Supplemental Material [41]). During dynamic dDAC loading, the pressure increased rapidly over a few tens of milliseconds, and then kept increasing at a lower rate (see Table I of the Supplemental Material). Data discussed in the following were acquired during the initial rapid compression, which always comprised the onset of the phase transition; compression rates were estimated via linear fitting of the P evolution in the examined interval (Fig. 2). In run 1, compression was performed at 2000 K, with an average compression rate of 400 GPa/s: run 2 reached 530 GPa/s at 1400 K. Run 3 and run 4 were performed at ambient temperature and reached compression rates of 360 GPa/s and 2.5 GPa/s, respectively. It should be noted that in run 4 the compression was performed without using the intermediate buffer. X-ray diffraction data were collected in situ during compression with sufficient temporal resolution for characterization of the structural evolution and accurate determination of the transition onset. During runs 1-3, XRD data were acquired at 2 ms/pattern, while the acquisition time was increased to 20 ms/pattern during run 4. For each experiment,

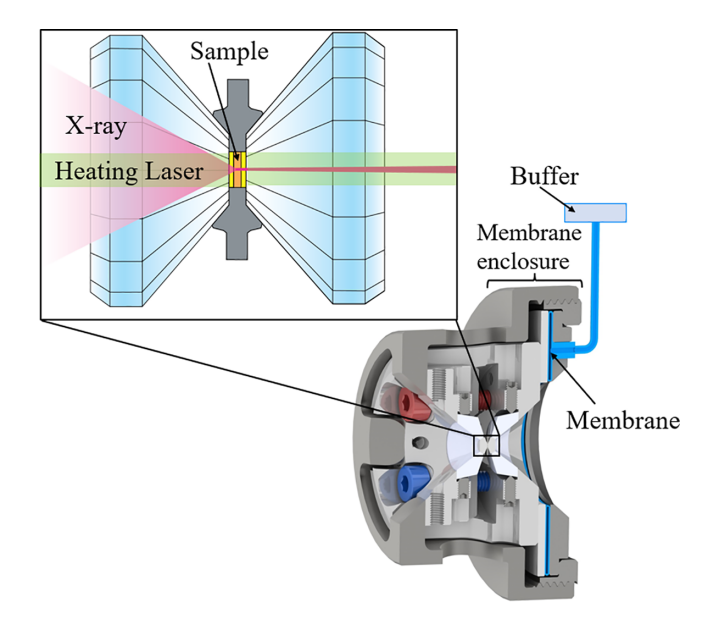


FIG. 1. Schematic view of the experimental setup used on the 13-IDD beamline at the APS synchrotron. Dynamic loading of the DAC was performed using a membrane and an enclosure compatible with the mini-BX80 cells; the intermediate buffer allowed to perform fast (ms) compression runs. The structure of the sample was monitored in real time using XRD. The x-ray beam was spatially overlapped with the laser-heating spot and had a wavelength of 0.3344 Å.

the sample was compressed statically up to a pressure value close to the phase boundary before launching the dynamic compression run, as to ensure observation of the onset of the transformation during loading.

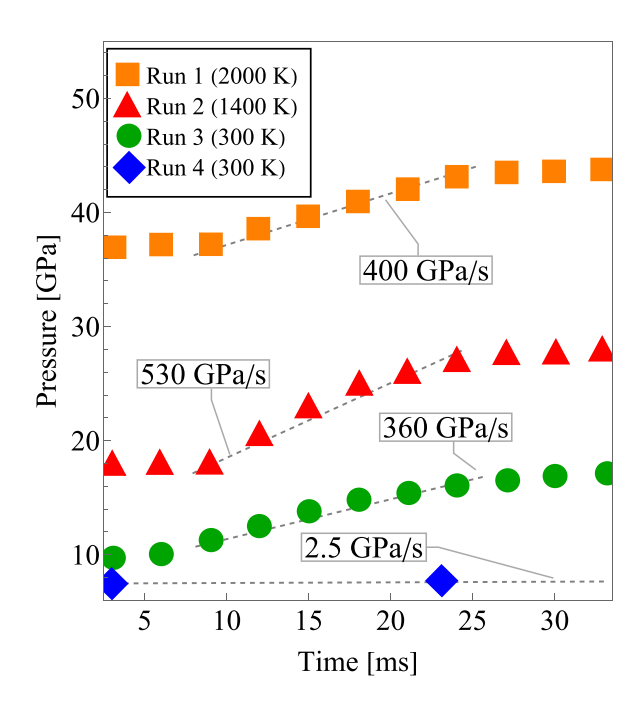


FIG. 2. Temporal evolution of pressure during dynamic loading for the four experimental runs; pressure was measured using the known EOS of KCl. For each run, temperature values, as well as compression rates, are reported; in run 4, no intermediate buffer was used, resulting in a  $\sim 100$  times lower compression rate.

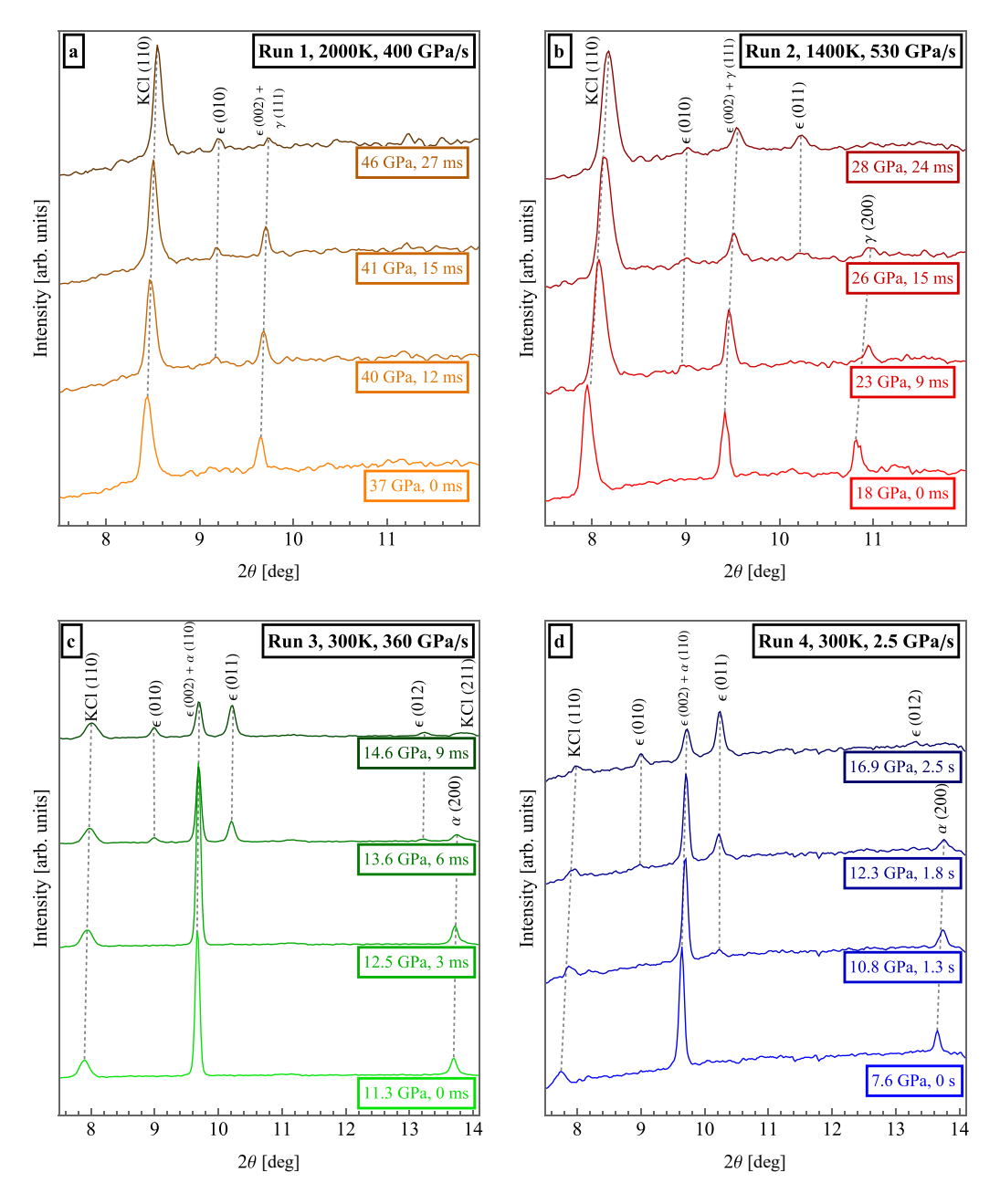


FIG. 3. Azimuthally integrated XRD patterns as a function of time show the structural changes in the sample upon compression. The XRD data is shown in the same colors used in Fig. 2 to represent pressure evolution. (a) and (b) HT experiments, showing the  $\gamma$ - $\epsilon$  transition at 2000 K and 1400 K, respectively. (c) and (d) Experiments at 300 K, showing the  $\alpha$ - $\epsilon$  transition for compression at 360 GPa/s and 2.5 GPa/s, respectively. For all patterns, the peaks of the observed Fe phases, as well as those of KCl, are indexed; the time values are measured with respect to the beginning of the dDAC compression run.

## III. RESULTS

In run 1 the sample was precompressed up to 37 GP, and temperature was increased up to 2000 K before dynamic loading [Fig. 3(a)]; at these initial conditions only the  $\gamma$  phase is present. During loading we observe the appearance of the  $\epsilon$ (010) reflection ( $\sim$ 9.2°) after 12 ms, at 40 GPa. Coexistence of the  $\gamma$  and  $\epsilon$  phases is observed up to 46 GPa, and progression of the transformation is confirmed by the changes in relative intensity of the correspondent peaks. At 46 GPa, the peak observed at  $\sim$ 9.7° can be indexed as either the  $\gamma$ (111) or the  $\epsilon$ (002) reflections. The crystalline texture, which can

be inferred by examining the intensity distribution along the Debye-Scherrer ring in the 2D XRD data, is more consistent with the  $\gamma$  phase (see also Sec. III C of the Supplemental Material). Moreover, based on previous experiments, the  $\epsilon$  phase is expected to grow along a preferred orientation in a DAC, which would result in a decrease of the intensity of  $\epsilon$ (002) reflection [42,43]. Thus, we do not expect to observe signal from the  $\epsilon$ (002) peak over the 2 ms integration time, and we interpret this peak as the signature of some residual  $\gamma$  phase. In run 2 the sample was precompressed up to 18 GPa and temperature was maintained at 1400 K during dynamic loading

[Fig. 3(b)]. At t = 0 ms, all the Fe peaks can be indexed as reflections from the  $\gamma$  phase. The  $\epsilon(010)$  peak becomes visible after 9 ms, at 23 GPa, and at 28 GPa, after 15 ms, the  $\gamma(200)$ reflection is no longer visible, leaving only the  $\gamma(111)$  peak overlapping with the  $\epsilon(002)$  peak in the diffraction pattern. In run 3 the sample was initially compressed to about 11 GPa, a pressure at which only the  $\alpha$  phase is present. Dynamic loading was performed at 300 K and 360 GPa/s [Fig. 3(c)]; at 13.6 GPa, we observe the appearance of the  $\epsilon(010)$ ,  $\epsilon(011)$ , and  $\epsilon(012)$  reflections. In run 4 compression was performed at 300 K without the use of the intermediate buffer, resulting in a compression rate reduction by a factor  $\sim 100$  to 2.5 GPa/s [Fig. 3(d)]. The sample was compressed statically up to 7 GPa, and at this compression rate the emergence of the  $\epsilon(010)$ and  $\epsilon(011)$  reflections was observed at pressures as low as 10.8 GPa, a value that is in agreement with the  $\alpha$ - $\epsilon$  phase boundary identified in static compression experiments [4]. It is worth noting that for all runs, despite persistence of small fractions of the initial phase during dynamic loading, the sample continues to compress slowly for several seconds. XRD collected after this period of slow compression confirmed that the sample had fully transformed into the  $\epsilon$  phase (see also Sec. III C of the Supplemental Material).

### IV. DISCUSSION

The experiments here presented using a dDAC apparatus to perform HP-HT experiments and reach compression rates up to  $\sim$ 500 GPa/s to investigate the influence of the loading timescale on Fe behavior at extreme conditions. Although these compression rates are much slower than those achieved in traditional shock compression experiments, they are several orders of magnitude higher than static compression studies at high temperature. Experimental runs performed at hundreds of GPa/s will be thus referred to as dynamic in order to stress the difference with previous experiments when comparing the results. The transition onsets measured at high compression rates for both the fcc-hcp  $(\gamma - \epsilon)$  and the bcc-hcp  $(\alpha - \epsilon)$  phase transitions of Fe are shown in Fig. 4 and overlaid with four previous results from static compression experiments that employ different experimental methods [4,8,9,11]. For the  $\gamma$ - $\epsilon$ transition, results from dDAC are in good agreement with the phase boundaries proposed by Shen et al. [4], while they exhibit a markedly lower transition onset compared with more recent static compression experiments, which are the current state-of-the-art reference for the equilibrium phase diagram [8,9]. It is worth noting that, independently of the considered reference for the equilibrium phase boundary, no increase in the phase transition onset is observed for the  $\gamma$ - $\epsilon$  transition under ms compression. In contrast, for a compression rate of 360 GPa/s at 300 K, the  $\alpha$ - $\epsilon$  transition is observed at 13.6 GPa, a higher pressure with respect to the boundary from static compression experiments. To confirm that the shift observed in the  $\alpha$ - $\epsilon$  transition is due to the compression timescale, we have performed an additional experiment (run 4, not shown in Fig. 4) at  $\sim$ 100 lower compression rate; the XRD data confirms that at 2.5 GPa/s the transition onset is 10.8 GPa, in much closer agreement with the equilibrium value. Interestingly, a similar trend has also been observed in recent laser-driven ramp compression experiments that re-

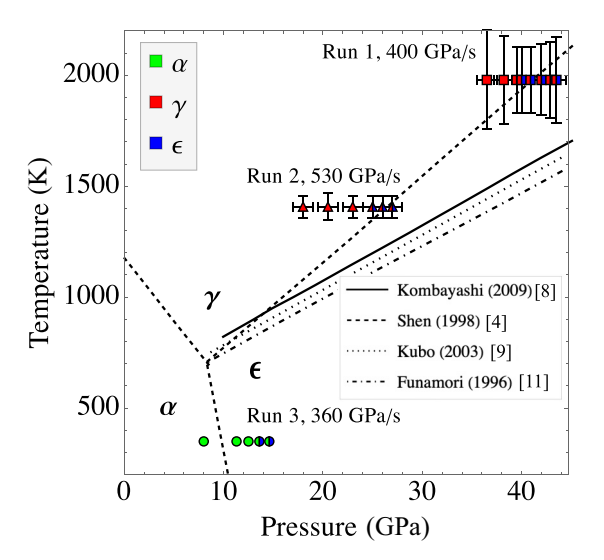


FIG. 4. Experimental results from dDAC experiments compared with the state-of-the-art equilibrium phase diagram of Fe. Data are represented using markers of different shapes for each run, while the colours correspond to different Fe phases. The solid line is the  $\gamma$ - $\epsilon$  equilibrium phase diagram in Kombayashi *et al.* [8]; the dotted lines represent the equilibrium boundary from other experimental studies, including the  $\alpha$ - $\epsilon$  boundary reported by Shen *et al.* [4,9,11].

ported a shift of the  $\alpha$ - $\epsilon$  transition onset with increasing strain rate [44]. Our results demonstrate the capability of the LH-dDAC apparatus to generate high pressures over timescales at which kinetic effects can be observed and characterized. Furthermore, we observe a different behavior of the  $\alpha$ - $\epsilon$  and  $\gamma$ - $\epsilon$  phase boundaries at high compression rates, with the transition onset being increased and lowered, respectively, compared to equilibrium phase diagram.

## A. Kinetic effects under dynamic compression

The influence of compression rate on HP phase transitions has already been analyzed in several systems; however, the effects of fast compression on the phase boundaries strongly depend on the system and on the specifics of the deformation mechanism. For example, in certain systems higher compression rates can cause an increase of the transition pressure, as the fast loading hinders the rearrangement of the atoms (so-called kinetic hindrance) [45]. In contrast, several systems have been observed to exhibit a phase transition lowering under shock-compression, e.g., silicon [46,47], bismuth [48], and antimony [49]. Interestingly, with the exception of silicon, the lowering in pressure is observed for displacive transitions, i.e., transformations that require no change in unit cell volume and happen via small displacements of the atoms.

Our results indicate two distinct trends in the  $\alpha$ - $\epsilon$  and  $\gamma$ - $\epsilon$  phase transitions of Fe under dynamic loading: compared to static compression experiments, the onset of  $\epsilon$  formation is increased and lowered, respectively. Though the two transition onsets may be influenced by thermal effects, we notice that temperature cannot fully explained the lowering of the  $\gamma$ - $\epsilon$  transition onset reported here. Based on previous results from dynamic compression experiments, this is likely due to differences in the transition mechanisms that govern

the transformations at the atomic level. The bcc-hcp ( $\gamma$ - $\epsilon$ ) transformation happens via a combination of compression along one axis and shuffle of the planes [29,30,50]; recent experiments have confirmed that the completion of the transformation requires two steps: a displacive seeding followed by a reconstructive (i.e., involving bond breaking) deformation [51]. Under dynamic compression, a reconstructive transformation is expected to exhibit kinetic hindrance, as also suggested by molecular dynamics simulations of the  $\alpha$ - $\epsilon$  transition [52]. On the other hand, the fcc and hcp structures are more closely related, as they only differ in the stacking of the planes along one direction; the transformation is thus expected to happen via a purely displacive deformation [53] that may not be affected by kinetic hindrance, and could thus explain the phase transition lowering observed here.

### V. CONCLUSIONS

In this study, we demonstrate dynamic compression of a material in a dDAC setup coupled with stable laser heating. Compression rates of hundreds of GPa/s were attained while simultaneously maintaining high temperatures up to 2000 K. Collection of time-resolved XRD data with millisecond time resolution enabled characterization of the phase transitions of Fe *in situ*. Interestingly, the dDAC laser-heating setup allows exploration of isothermal compression of a material, a pathway not attainable using conventional shock-compression techniques. This demonstrates a new approach for exploration of HP-HT phase transitions under dynamic loading. With this approach, we provide insight on the  $\gamma$ - $\epsilon$  phase transition of Fe under dynamic compression, and compare our results with those obtained for the  $\alpha$ - $\epsilon$  transition, as well as the equilibrium

phase diagram. We observe that the increase in compression rate affects the phase transitions of Fe differently, and we attribute the differences to the specific deformation mechanisms. Indeed, no sign of kinetic hindrance is observed for the displacive  $\gamma$ - $\epsilon$  phase transition up to 500 GPa/s. In contrast, the reconstructive  $\alpha$ - $\epsilon$  transition exhibits a marked increase of the transition onset with the compression rate. Thus, particular care should be taken when using experimental data to model extreme conditions processes at different timescales.

#### ACKNOWLEDGMENTS

This work was carried out at the GeoSoilEnviroCARS (The University of Chicago, Sector 13), Advanced Photon Source (Argonne National Laboratory). Experiment allocated for GUP 74511 (PI: Pandolfi). GeoSoilEnviroCARS is supported by the National Science Foundation (NSF)-Earth Sciences (No. EAR-1634415). The Advanced Photon Source is a U.S. Department of Energy (DOE) Office of Science User Facility operated for the DOE Office of Science by Argonne National Laboratory under Contract No. DE-AC02-06CH11357. A.E.G., R.L.S., and S.P. acknowledge support from 2019 DOE FES ECA. A.E.G. and W.L.M. acknowledge support by the Geophysics Program at NSF (EAR2049620). M.R. acknowledges support from the College of Physical and Mathematical Sciences at Brigham Young University. This work was supported in part by the U.S. Department of Energy, Office of Science, Office of Workforce Development for Teachers and Scientists (WDTS) under the Science Undergraduate Laboratory Internships (SULI) program at SLAC National Accelerator Laboratory.

- [1] J. Monteux and J. Arkani-Hamed, Shock wave propagation in layered planetary interiors: Revisited, Icarus **331**, 238 (2019).
- [2] Y. L. Godec, A. Courac, and V. L. Solozhenko, High-pressure synthesis of superhard and ultrahard materials, J. Appl. Phys. 126, 151102 (2019).
- [3] T. S. Duffy and R. F. Smith, Ultra-high pressure dynamic compression of geological materials, Front. Earth Sci. 7, 23 (2019).
- [4] G. Shen, H.- kwang Mao, R. J. Hemley, T. S. Duffy, and M. L. Rivers, Melting and crystal structure of iron at high pressures and temperatures, Geophys. Res. Lett. **25**, 373 (1998).
- [5] O. L. Anderson, Properties of iron at the Earth's core conditions, Geophys. J. R. Astron. Soc. 84, 561 (1986).
- [6] A. Dewaele, B. Amadon, A. Bosak, V. Svitlyk, and F. Occelli, Synthesis of single crystals of  $\epsilon$ -iron and direct measurements of its elastic constants, Phys. Rev. Lett. **131**, 034101 (2023).
- [7] R. Boehler, Temperatures in the Earth's core from melting-point measurements of iron at high static pressures, Nature (London) **363**, 534 (1993).
- [8] T. Komabayashi, Y. Fei, Y. Meng, and V. Prakapenka, In-situ x-ray diffraction measurements of the γ-ε transition boundary of iron in an internally-heated diamond anvil cell, Earth Planet. Sci. Lett. 282, 252 (2009).
- [9] A. Kubo, E. Ito, T. Katsura, T. Shinmei, H. Yamada, O. Nishikawa, M. Song, and K. Funakoshi, In situ X-ray observation of iron using Kawai-type apparatus equipped with sintered

- diamond: Absence of  $\beta$  phase up to 44 GPa and 2100 K, Geophys. Res. Lett. **30**, 1126 (2003).
- [10] Y. Ma, M. Somayazulu, G. Shen, H.- kwang Mao, J. Shu, and R. J. Hemley, In situ x-ray diffraction studies of iron to Earth-core conditions, Phys. Earth Planet. Inter. 143-144, 455 (2004).
- [11] N. Funamori, T. Yagi, and T. Uchida, High-pressure and high-temperature in situ x-ray diffraction study of iron to above 30 GPa using MA8-type apparatus, Geophys. Res. Lett. 23, 953 (1996)
- [12] F. Miozzi, J. Matas, N. Guignot, J. Badro, J. Siebert, and G. Fiquet, A new reference for the thermal equation of state of iron, Minerals 10, 100 (2020).
- [13] D. Bancroft, E. L. Peterson, and S. Minshall, Polymorphism of iron at high pressure, J. Appl. Phys. **27**, 291 (1956).
- [14] R. A. Fischer and A. J. Campbell, The axial ratio of hcp Fe and Fe-Ni-Si alloys to the conditions of Earth's inner core, Am. Mineral. 100, 2718 (2015).
- [15] K. Ohta, Y. Nishihara, Y. Sato, K. Hirose, T. Yagi, S. I. Kawaguchi, N. Hirao, and Y. Ohishi, An experimental examination of thermal conductivity anisotropy in hcp iron, Front. Earth Sci. 6, 176 (2018).
- [16] C. S. Yoo, N. C. Holmes, M. Ross, D. J. Webb, and C. Pike, Shock temperatures and melting of iron at Earth core conditions, Phys. Rev. Lett. 70, 3931 (1993).

- [17] A. Benuzzi-Mounaix, M. Koenig, G. Huser, B. Faral, D. Batani, E. Henry, M. Tomasini, B. Marchet, T. A. Hall, M. Boustie, T. De Rességuier, M. Hallouin, F. Guyot, D. Andrault, and T. Charpin, Absolute equation of state measurements of iron using laser driven shocks, Phys. Plasmas 9, 2466 (2002).
- [18] Y. Ping, F. Coppari, D. G. Hicks, B. Yaakobi, D. E. Fratanduono, S. Hamel, J. H. Eggert, J. R. Rygg, R. F. Smith, D. C. Swift, D. G. Braun, T. R. Boehly, and G. W. Collins, Solid iron compressed up to 560 GPa, Phys. Rev. Lett. 111, 065501 (2013).
- [19] N. Amadou, E. Brambrink, T. Vinci, A. Benuzzi-Mounaix, G. Huser, S. Brygoo, G. Morard, F. Guyot, T. de Resseguier, S. Mazevet, K. Miyanishi, N. Ozaki, R. Kodama, O. Henry, D. Raffestin, T. Boehly, and M. Koenig, Probing iron at super-Earth core conditions, Phys. Plasmas 22, 022705 (2015).
- [20] M. Harmand, A. Ravasio, S. Mazevet, J. Bouchet, A. Denoeud, F. Dorchies, Y. Feng, C. Fourment, E. Galtier, J. Gaudin, F. Guyot, R. Kodama, M. Koenig, H. J. Lee, K. Miyanishi, G. Morard, R. Musella, B. Nagler, M. Nakatsutsumi, N. Ozaki et al., X-ray absorption spectroscopy of iron at multimegabar pressures in laser shock experiments, Phys. Rev. B 92, 024108 (2015).
- [21] A. Denoeud, N. Ozaki, A. Benuzzi-Mounaix, H. Uranishi, Y. Kondo, R. Kodama, E. Brambrink, A. Ravasio, M. Bocoum, J.-M. Boudenne, M. Harmand, F. Guyot, S. Mazevet, D. Riley, M. Makita, T. Sano, Y. Sakawa, Y. Inubushi, G. Gregori, M. Koenig *et al.*, Dynamic x-ray diffraction observation of shocked solid iron up to 170 GPa, Proc. Natl. Acad. Sci. USA 113, 7745 (2016).
- [22] R. Torchio, F. Occelli, O. Mathon, A. Sollier, E. Lescoute, L. Videau, T. Vinci, A. Benuzzi-Mounaix, J. Headspith, W. Helsby, S. Bland, D. Eakins, D. Chapman, S. Pascarelli, and P. Loubeyre, Probing local and electronic structure in warm dense matter: single pulse synchrotron x-ray absorption spectroscopy on shocked Fe, Sci. Rep. 6, 26402 (2016).
- [23] S. Merkel, S. Hok, C. Bolme, D. Rittman, K. J. Ramos, B. Morrow, H. J. Lee, B. Nagler, E. Galtier, E. Granados, A. Hashim, W. L. Mao, and A. E. Gleason, Femtosecond Visualization of hcp-iron strength and plasticity under shock compression, Phys. Rev. Lett. 127, 205501 (2021).
- [24] B. Branch and B. J. Jensen, Dynamic x-ray diffraction to study the shock-induced  $\alpha$ - $\epsilon$  phase transition in iron, AIP Conf. Proc. **1979**, 040001 (2018).
- [25] J. C. Boettger and D. C. Wallace, Metastability and dynamics of the shock-induced phase transition in iron, Phys. Rev. B **55**, 2840 (1997).
- [26] J. A. Hawreliak, D. H. Kalantar, J. S. Stölken, B. A. Remington, H. E. Lorenzana, and J. S. Wark, High-pressure nanocrystalline structure of a shock-compressed single crystal of iron, Phys. Rev. B 78, 220101(R) (2008).
- [27] S. Singh, R. Briggs, M. G. Gorman, L. X. Benedict, C. J. Wu, S. Hamel, A. L. Coleman, F. Coppari, A. Fernandez-Panella, C. McGuire, M. Sims, J. K. Wicks, J. H. Eggert, D. E. Fratanduono, and R. F. Smith, A structural study of hcp and liquid iron under shock compression up to 275 GPa, arXiv:2304.07933.
- [28] R. F. Smith, J. H. Eggert, R. Jeanloz, T. S. Duffy, D. G. Braun, J. R. Patterson, R. E. Rudd, J. Biener, A. E. Lazicki, A. V. Hamza, J. Wang, T. Braun, L. X. Benedict, P. M. Celliers, and

- G. W. Collins, Ramp compression of diamond to five terapascals, Nature (London) **511**, 330 (2014).
- [29] J. Hawreliak, J. D. Colvin, J. H. Eggert, D. H. Kalantar, H. E. Lorenzana, J. S. Stölken, H. M. Davies, T. C. Germann, B. L. Holian, K. Kadau, P. S. Lomdahl, A. Higginbotham, K. Rosolankova, J. Sheppard, and J. S. Wark, Analysis of the x-ray diffraction signal for the  $\alpha$ - $\epsilon$  transition in shock-compressed iron: Simulation and experiment, Phys. Rev. B **74**, 184107 (2006).
- [30] D. H. Kalantar, J. F. Belak, G. W. Collins, J. D. Colvin, H. M. Davies, J. H. Eggert, T. C. Germann, J. Hawreliak, B. L. Holian, K. Kadau, P. S. Lomdahl, H. E. Lorenzana, M. A. Meyers, K. Rosolankova, M. S. Schneider, J. Sheppard, J. S. Stölken, and J. S. Wark, Direct observation of the  $\alpha$ - $\epsilon$  transition in shock-compressed iron via nanosecond x-ray diffraction, Phys. Rev. Lett. **95**, 075502 (2005).
- [31] J. A. Hawreliak and S. J. Turneaure, Probing the lattice structure of dynamically compressed and released single crystal iron through the alpha to epsilon phase transition, J. Appl. Phys. 129, 135901 (2021).
- [32] J. A. Hawreliak and S. J. Turneaure, Observations of twinning microstructure in iron ramp-compressed through the  $\alpha$ - $\epsilon$  phase transition, Phys. Rev. B **106**, 174306 (2022).
- [33] J. Wang, R. F. Smith, J. H. Eggert, D. G. Braun, T. R. Boehly, J. R. Patterson, P. M. Celliers, R. Jeanloz, G. W. Collins, and T. S. Duffy, Ramp compression of iron to 273 GPa, J. Appl. Phys. 114, 023513 (2013).
- [34] R. F. Smith, D. E. Fratanduono, D. G. Braun, T. S. Duffy, J. K. Wicks, P. M. Celliers, S. J. Ali, A. Fernandez-Pañella, R. G. Kraus, D. C. Swift, G. W. Collins, and J. H. Eggert, Equation of state of iron under core conditions of large rocky exoplanets, Nat. Astron. 2, 452 (2018).
- [35] R. G. Kraus, R. J. Hemley, S. J. Ali, J. L. Belof, L. X. Benedict, J. Bernier, D. Braun, R. E. Cohen, G. W. Collins, F. Coppari, M. P. Desjarlais, D. Fratanduono, S. Hamel, A. Krygier, A. Lazicki, J. Mcnaney, M. Millot, P. C. Myint, M. G. Newman, J. R. Rygg *et al.*, Measuring the melting curve of iron at super-Earth core conditions, Science 375, 202 (2022).
- [36] S. V. Sinogeikin, J. S. Smith, E. Rod, C. Lin, C. Kenney-Benson, and G. Shen, Online remote control systems for static and dynamic compression and decompression using diamond anvil cells, Rev. Sci. Instrum. 86, 072209 (2015).
- [37] Z. Jenei, H. P. Liermann, R. Husband, A. S. J. Méndez, D. Pennicard, H. Marquardt, E. F. O'Bannon, A. Pakhomova, Z. Konopkova, K. Glazyrin, M. Wendt, S. Wenz, E. E. McBride, W. Morgenroth, B. Winkler, A. Rothkirch, M. Hanfland, and W. J. Evans, New dynamic diamond anvil cells for tera-pascal per second fast compression x-ray diffraction experiments, Rev. Sci. Instrum. 90, 065114 (2019).
- [38] Z. Konôpková, A. Rothkirch, A. K. Singh, S. Speziale, and H.-P. Liermann, In situ x-ray diffraction of fast compressed iron: Analysis of strains and stress under non-hydrostatic pressure, Phys. Rev. B **91**, 144101 (2015).
- [39] G. Shen, V. B. Prakapenka, P. J. Eng, M. L. Rivers, and S. R. Sutton, Facilities for high-pressure research with the diamond anvil cell at GSECARS, J. Synchrotron Radiat. 12, 642 (2005).
- [40] V. B. Prakapenka, A. Kubo, A. Kuznetsov, A. Laskin, O. Shkurikhin, P. Dera, M. L. Rivers, and S. R. Sutton, Advanced flat top laser heating system for high pressure research at GSE-

- CARS: application to the melting behavior of germanium, High Press. Res. **28**, 225 (2008).
- [41] See Supplemental Material at http://link.aps.org/supplemental/ 10.1103/PhysRevResearch.6.013316 for a description of the experimental method and data processing. There is also an explaination of the error bar calculations, a description of the temperature determinations, and discussions on sample texture and hydrostaticity in the high pressure cell.
- [42] A. K. Singh, A. Jain, H. P. Liermann, and S. K. Saxena, Strength of iron under pressure up to 55 GPa from x-ray diffraction line-width analysis, J. Phys. Chem. Solids 67, 2197 (2006).
- [43] S. Merkel, A. Lincot, and S. Petitgirard, Microstructural effects and mechanism of bcc-hcp-bcc transformations in polycrystalline iron, Phys. Rev. B **102**, 104103 (2020).
- [44] N. Amadou, T. de Resseguier, E. Brambrink, T. Vinci, A. Benuzzi-Mounaix, G. Huser, G. Morard, F. Guyot, K. Miyanishi, N. Ozaki, R. Kodama, and M. Koenig, Kinetics of the iron  $\alpha$ - $\epsilon$  phase transition at high-strain rates: Experiment and model, Phys. Rev. B **93**, 214108 (2016).
- [45] R. J. Husband, E. F. O'Bannon, H.-P. Liermann, M. J. Lipp, A. S. J. Méndez, Z. Konôpková, E. E. Mcbride, W. J. Evans, and Z. Jenei, Compression-rate dependence of pressure-induced phase transitions in Bi, Sci. Rep. 11, 14859 (2021).
- [46] E. E. McBride, A. Krygier, A. Ehnes, E. Galtier, M. Harmand, Z. Konôpková, H. J. Lee, H.-P. Liermann, B. Nagler, A. Pelka, M. Rödel, A. Schropp, R. F. Smith, C. Spindloe, D. Swift, F. Tavella, S. Toleikis, T. Tschentscher, J. S. Wark, and A. Higginbotham, Phase transition lowering in dynamically compressed silicon, Nat. Phys. 15, 89 (2019).

- [47] S. Pandolfi, S. B. Brown, P. G. Stubley, A. Higginbotham, C. A. Bolme, H. J. Lee, B. Nagler, E. Galtier, R. L. Sandberg, W. Yang, W. L. Mao, J. S. Wark, and A. E. Gleason, Atomistic deformation mechanism of silicon under laser-driven shock compression, Nat. Commun. 13, 5535 (2022).
- [48] C. M. Pépin, A. Sollier, A. Marizy, F. Occelli, M. Sander, R. Torchio, and P. Loubeyre, Kinetics and structural changes in dynamically compressed bismuth, Phys. Rev. B 100, 060101(R) (2019).
- [49] A. L. Coleman, M. G. Gorman, R. Briggs, R. S. McWilliams, D. McGonegle, C. A. Bolme, A. E. Gleason, D. E. Fratanduono, R. F. Smith, E. Galtier, H. J. Lee, B. Nagler, E. Granados, G. W. Collins, J. H. Eggert, J. S. Wark, and M. I. McMahon, Identification of phase transitions and metastability in dynamically compressed antimony using ultrafast x-ray diffraction, Phys. Rev. Lett. 122, 255704 (2019).
- [50] R. Fréville, A. Dewaele, N. Bruzy, V. Svitlyk, and G. Garbarino, Comparison between mechanisms and microstructures of  $\alpha$ - $\gamma$ ,  $\gamma$ - $\epsilon$ , and  $\alpha$ - $\epsilon$ - $\alpha$  phase transitions in iron, Phys. Rev. B **107**, 104105 (2023).
- [51] E. Boulard, C. Denoual, A. Dewaele, A. King, Y. Le Godec, and N. Guignot, Following the phase transitions of iron in 3D with x-ray tomography and diffraction under extreme conditions, Acta Mater. 192, 30 (2020).
- [52] J.-L. Shao, P. Wang, F.-G. Zhang, and A.-M. He, Hcp/fcc nucleation in bcc iron under different anisotropic compressions at high strain rate: Molecular dynamics study, Sci. Rep. 8, 7650 (2018).
- [53] G. B. Olson and M. Cohen, A general mechanism of martensitic nucleation: Part I. General concepts and the FCC → HCP transformation, Metall. Trans. A 7, 1897 (1976).